Two complementary codes in the superior colliculus differentiate external from self-generated spatial features

Suma Chinta and Scott R. Pluta, Department of Biology, Purdue University, West Lafayette, IN

Abstract

Spatial awareness is often intentional, arising from deliberate movements towards a target, while at other times it emerges from unexpected motion in the scene. While navigating the environment, animals must differentiate the spatial cues generated by self-motion from object movements that originate externally. To reveal the neural basis of this ability, we examined the midbrain superior colliculus (SC), which contains multiple egocentric maps of sensorimotor space. By simulating whisker-guided navigation through a dynamic landscape, we discovered a transient neural response that selectively emerged for unexpected, externally generated tactile motion. This transient response only emerged when external motion engaged different whiskers, arguing that sensorimotor expectations are specific to a somatotopic location. When external motion engaged the same whiskers, neurons shifted their spike timing to match self-generated spatial features. Thus, representations based on the timing of self-generated cues may surpass the spatial acuity of the whisker array. In conclusion, the SC contains complementary rate and temporal codes to differentiate external from self-generated tactile features.

Introduction

Navigation is an active process involving the integration of self-generated spatial cues. For example, humans move their eyes to visualize a scene or stroke a surface to feel its contour. While moving through space, animals must differentiate the expected consequences of their actions, induced by active sensing, from unexpected motion in the environment. What are the neural mechanisms underlying this spatial awareness?

To answer this question, we focused on the midbrain superior colliculus (SC), which contains multiple egocentric maps of sensorimotor space (Allen et al., 2021; Drager and Hubel, 1976; Hikosaka and Wurtz, 1985; Munoz and Wurtz, 1993). Many SC mediated behaviors involve spatial processing, such as pursuing prey, escaping predators, or simply orienting towards the appropriate object (Duan et al., 2021; Essig et al., 2021; Evans et al., 2018; Hoy et al., 2016; Huang et al., 2021; Shang et al., 2019). While visually tracking an object, the SC helps stabilize the visual field and adjust for discrepancies between the intended and the actual outcome of motor actions (Kojima and Soetedjo, 2018; Sommer and Wurtz, 2002). Given these insights, we

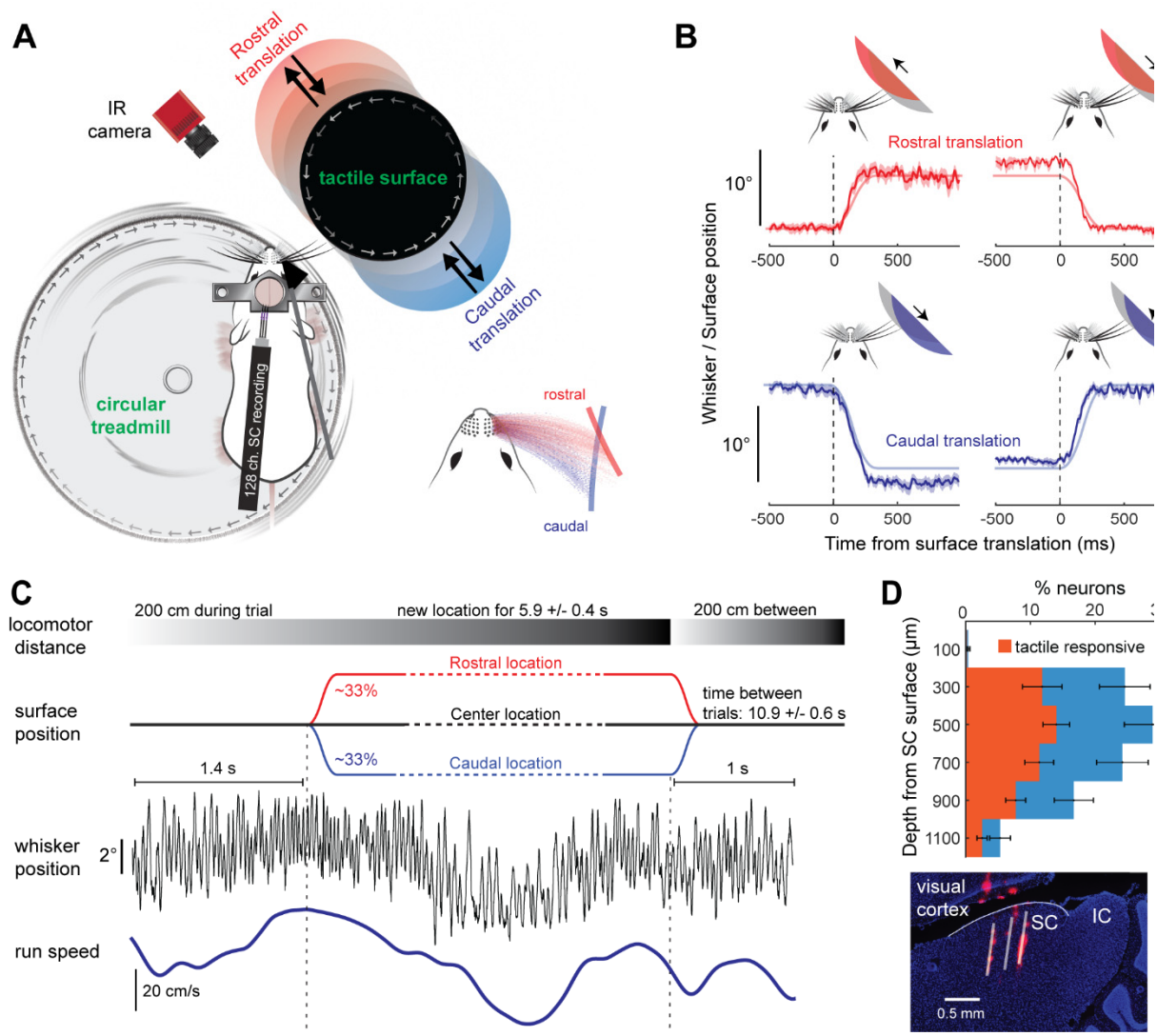

Figure 1. Tactile dynamics during whisker guided virtual navigation
A) Schematic of whisker guided virtual navigation, illustrating a head-fixed mouse locomoting on a treadmill and whisking against a surface. After trial initiation, there was an equal probability for the tactile surface to translate into either rostral (in red) or caudal (in blue) whisker space or staying at the center position (in black). Bottom right: single-whisker location density while the surface was at the rostral or caudal location. **B**) Whisker position (mean ± s.e.m) and surface location (transparent line) during rostral (top in red) and caudal (bottom in blue) translations. The first half is surface excursion while second half is the return to the center position. **C**) Trial structure aligning surface position, whisker position, and locomotion speed. **D**) Top: Percentage of tactile responsive SC neurons (orange) and total recorded neurons (blue) at various depths from the SC surface (12 mice, 873 neurons). Bottom: dye labeling of the electrode shanks in the intermediate and deep layers of the lateral SC.

hypothesized that SC neurons contain a code for differentiating external from self-generated spatial features. Since the SC is also important for visualizing stationary targets (Munoz and Wurtz, 1993), we anticipated finding a complementary code that supports stable representations

in the absence of external motion.While decades of research have outlined SC function during visuospatial processing, surprisingly less is known in the context of somatosensation (Basso and May, 2017; Cang et al., 2018; Nagy et al., 2006). The mouse SC is known to encode whisker stimuli, yet nearly all published work in this area has been performed under anesthesia (Bezdudnaya and Castro-Alamancos, 2011; Castro-Alamancos and Favero, 2016; Cohen et al., 2008; Cohen and Castro-Alamancos, 2010; Drager and Hubel, 1976). These experiments reveal that the SC contains a somatotopic map of whisker space, whereby individual neurons possess large (multi-whisker) receptive fields that are sensitive to whisker motion.

Sensory responses in the SC have primarily been characterized with a fixed sensor array (Basso and May, 2017; Cang et al., 2018). While this approach has been invaluable for segregating sensory from motor activity, it cannot reveal the neural mechanisms for distinguishing external and self-generated stimulation. The somatosensory whisker system offers a tractable model for answering this question, since mice actively palpate objects, and the precise dynamics of touch can be accurately determined using high-speed imaging and markerless tracking (Mathis et al., 2018).

To determine the neural basis of active somatosensation in the SC, we designed an experiment that mimics whisker-guided navigation. While running on a treadmill, mice rhythmically touched a cylindrical surface that rotated at the same velocity as their locomotion. This created a tactile flow-field that simulates running along a wall, in a manner similar to visual flow. Periodically, the flow-field translated along the mouse's horizontal axis, effectively changing the surface contour against the whiskers. Using spike times from populations of SC neurons, we accurately decoded surface location, with the highest accuracy for movements that engaged different whiskers. A transient response selectively emerged for externally generated tactile motion that habituated in a context-specific manner. The timing of spikes relative to self-generated tactile features generated a stable representation of object location.

Results

Whisker-guided virtual navigation

To mimic whisker-guided navigation, a head-fixed mouse whisked against a tactile surface that rotated at the same velocity as its locomotion (**Fig. 1A**). A high-speed (500fps) infrared camera and digital encoders recorded whisker kinematics, surface location, and running speed while an opaque flag and white noise obscured visual and auditory cues. After the mouse initiated a trial by running a set distance, the tactile surface would either translate rostrally, caudally or remain

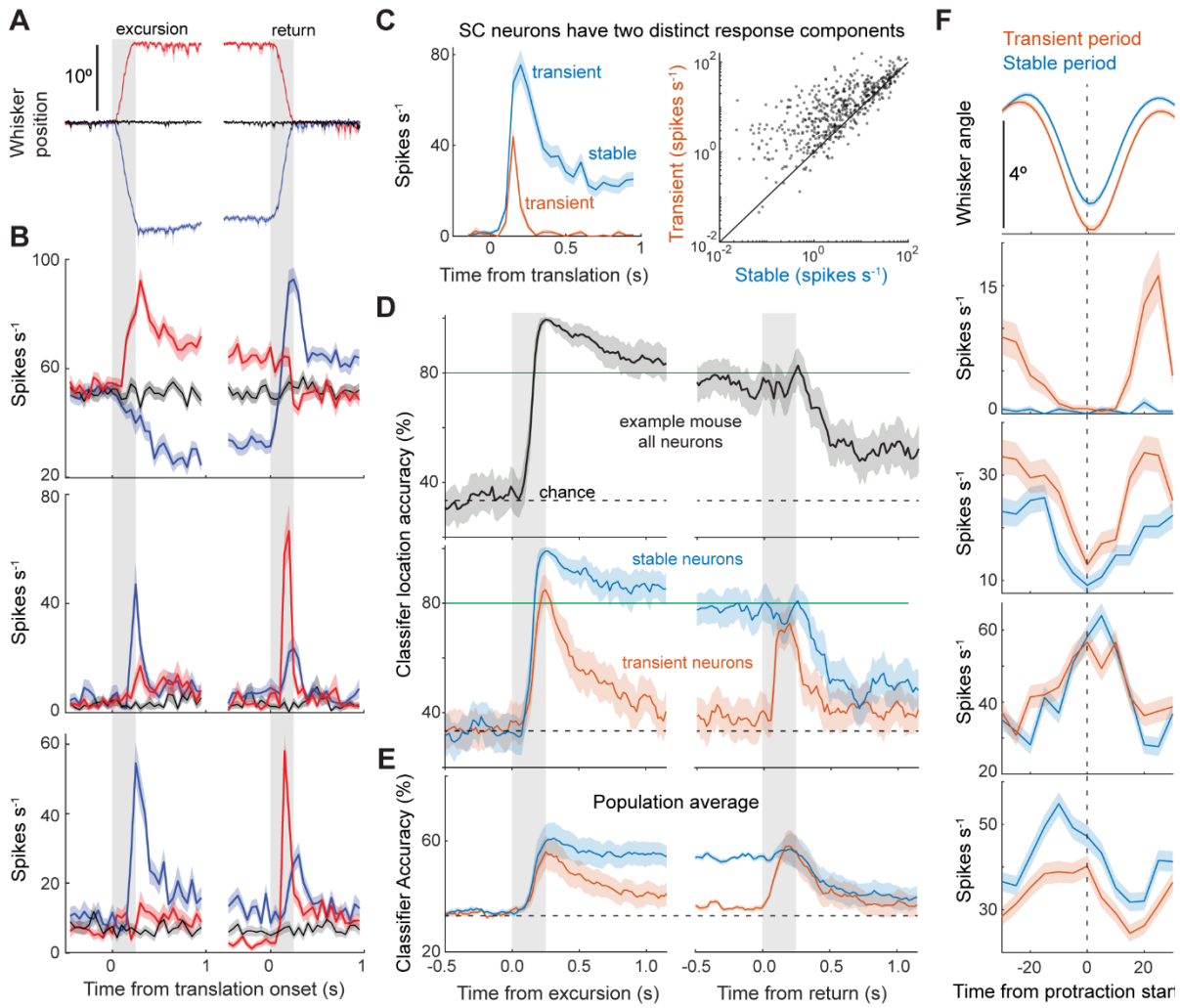

Figure 2. Superior colliculus accurately encodes surface location across multiple timescales **A**) Top: Trial averaged whisker position during rostral (red), center (black) and caudal (blue) translations in an example experiment. **B**) Histograms of firing rates for three example neurons in the same experiment. Grey shaded regions represent the surface translation periods. **C**) Left, two example neurons illustrating the distinct transient and stable response components evoked during surface translation. Right, scatter plot comparing the transient and stable firing rates of SC neurons (10 mice, 529 neurons). **D**) Top, neural decoding of surface location over time using all neurons recorded from one experiment (76 neurons, black trace). Bottom, same as above but using the stable neurons (30 neurons, red) or the transient neurons (46 neurons, blue). The black dashed line indicates the chance decoder performance of 1/3rd correct. **E**) Population averaged neural decoding for all stable and transient neurons (12 mice). **F**) Top, whisker angle aligned to the start of protraction. Bottom, firing rates of four example neurons aligned to the start of whisker protraction. Firing rates were plotted separately for the transient (blue) and stable (orange) response periods. All values are mean ± s.e.m.

at the starting location with equal probability. After staying at the new location for a set locomotor distance (if applicable), the surface would then return to the starting location. While running, mice adapted the position of their whiskers to track changes in surface location (**Fig. 1B**). Since translation timing was determined by locomotor distance, variation in locomotion

speed made translation onset somewhat unpredictable (**Fig. 1C**). A 3-shank, 128-channel silicon probe recorded neural activity simultaneously across the intermediate and deep layers of the lateral SC, approximately 300 – 1000 microns below its surface (**Fig. 1D**, 12 mice, 873 neurons). About two-thirds of all SC neurons displayed a significant response to surface translation (67 ± 6%, 12 mice, 578 neurons, $p < 0.05$, 1-way ANOVA).

The superior colliculus encodes external motion with transient and stable changes in firing rate

SC neurons responded to surface translation with distinct changes in firing rate that enabled accurate decoding of surface location. With the surface in the center (starting) location, baseline firing rates among neurons were mixed, ranging from less than one to more than 50 per second. During surface translation into a new location (**Fig. 2A**), the firing rate of most neurons rapidly increased while others decreased, as shown in three example units (**Fig. 2B**). Interestingly, neuronal firing rates were unique for each trajectory of motion and had two distinct response components. We classified these response components as 'transient' (TR, rapidly adapting response) or 'stable' (SR, sustained response) based on their rate and magnitude of adaptation (**Fig. 2C, Supp. Fig. 1D,** 30 ± 3% TR only, 53 ± 3% SR, see methods). To understand the information content among these neuron types, we tested the localization accuracy of population-level SC activity over time. Using a statistical classifier, we discovered that SC activity accurately encoded surface location, with the highest performance around the translation period, as shown in one example mouse (**Fig. 2D**, 99% accuracy, 76 total neurons). Classification accuracy for stable neurons was high for as long as the object remained in the new location, suggesting a stable representation of stimulus information (30 neurons, 1 mouse). After the surface returned to the center position, the firing rate of some neurons slowly returned to baseline (see **Fig. 2B**, top blue), as evident in the above-chance levels of classifier performance for this period (**Fig. 2D**, top right). On the other hand, performance for transient neurons was accurate only during external motion, due to their rapid adaptation rates (46 neurons, 1 mouse). This general trend was consistent across our population of mice, despite some heterogeneity in overall classifier performance (**Fig. 2E**, 68 ± 5% accuracy, 12 mice, and 475 neurons). To complement our statistical classifier, we calculated location modulation indices (**Suppl. Fig. 1A, B**), and found that neural populations displaying the largest response differences between rostral and caudal locations also had the highest classification accuracies (**Suppl. Fig. 1C**). Transient and stable firing rates were somatosensory in origin, since the

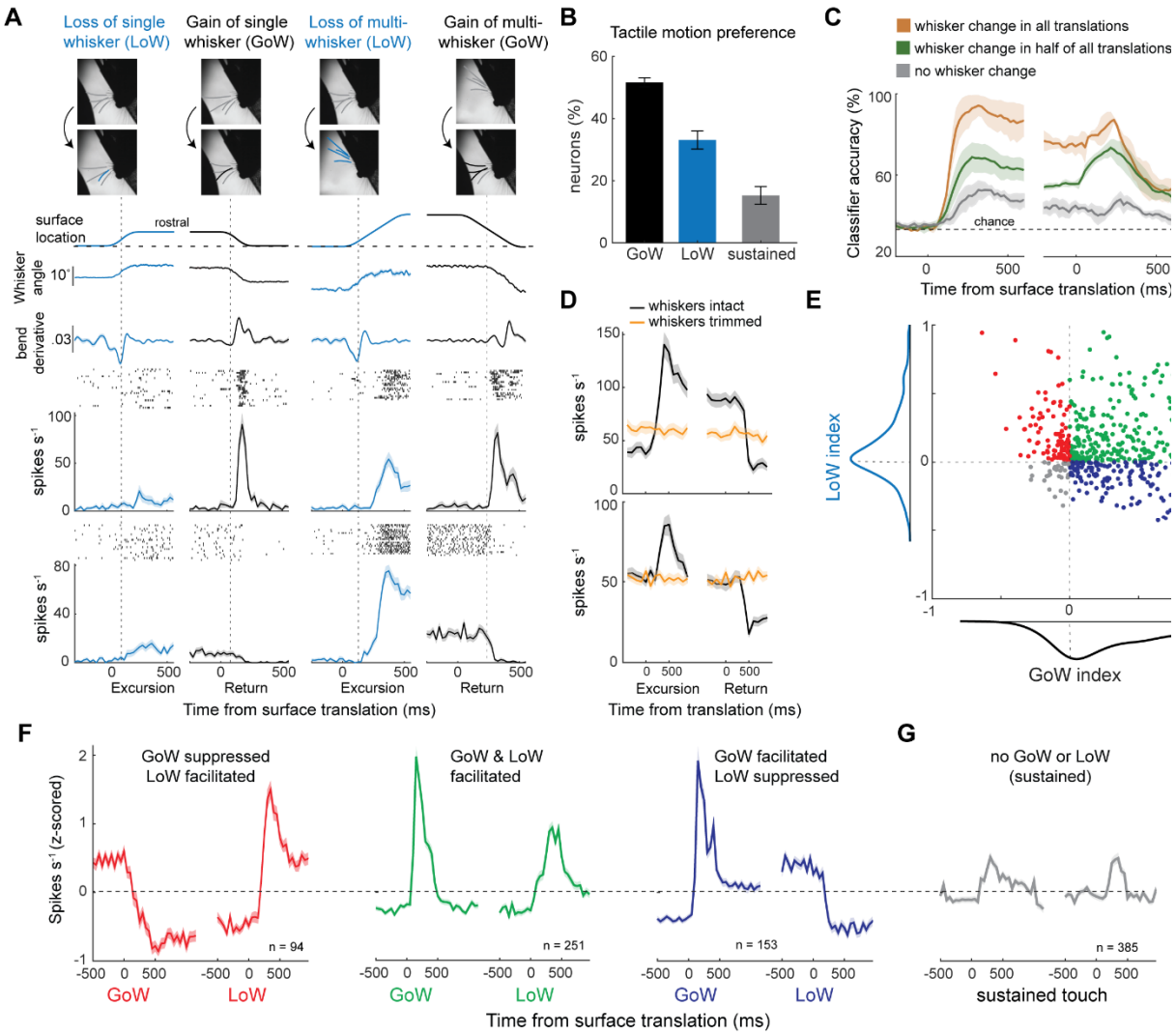

Figure 3. Gains and losses in whisker contact drive transient increases in spike rate
A) Surface location, whisker angle, whisker bend derivative, and the firing rates of two example neurons during gains (black) and losses (blue) in whisker touch. Dashed line marks the estimated moment of whisker change, based on whisker kinematics. The two bottom rows are example neurons, and each column is a unique change in whisker space indicated at the top. **B**) Percentage of neurons that preferred a gain of whisker contact (GoW, 52 ± 1%), loss of whisker contact (LoW, 33 ± 3%), or sustained touch (15 ± 3%, 6 mice, 336 neurons). **C**) Neural decoding of surface location when all translations contacted different whiskers (orange, 2 mice, 94 ± 5%), half of the translations contacted different whiskers (green, 6 mice, 71 ± 7%), and when all translations sustained contact with same whiskers (gray, 4 mice, 56 ± 3%). Dashed line is chance accuracy of 33%. **D**) The firing rate of two example neurons during whisker change with intact whiskers and after all the whiskers were trimmed off. **E**) Scatter plot comparing the normalized GoW and LoW responses of each neuron (10 mice, 529 neurons). **F**) Population averaged, z-scored firing rates of neurons grouped by the sign (+/-) of their response to GoW and LoW. **G**) Population averaged, z-scored firing rates of neurons during translations that sustained contact with the same whiskers (excursion and return, 8 mice, 385 neurons). All values are mean ± s.e.m.

temporal dynamics of spiking often aligned with whisker motion, in both the transient and stable periods of the trial, as shown in four example neurons (**Fig. 2F**).

Gains and losses in whisker contact drive accurate representations of surface location

To reveal the stimulus variables driving SC responses, we examined the dynamics of whisker touch during external motion. We discovered that external motion elicited large changes in firing rate only when whiskers gained (GoW) or lost (LoW) contact with the surface (**Fig. 3A**). The addition or subtraction of a single whisker from the surface was sufficient for this effect. Most neurons preferentially responded to whisker addition (GoW, 52 ± 1%, 6 mice, 336 neurons, **Fig. 3B**), while only a small percentage of neurons preferred surface translations that engaged the same whiskers at both locations (15 ± 3%, 6 mice, 336 neurons). Accordingly, neural decoding of surface location was much higher during translations that engaged different whiskers (GoW/LoW in all translations, 2 mice, 94 ± 5%, GoW/LoW in half of translations, 6 mice, 71 ± 7%), relative to translations that sustained touch with the same whiskers (4 mice, 56 ± 3%, **Fig. 3C**). In two mice, we repeated the experiment after trimming the whiskers and found that nearly all neurons lost their responsiveness to surface translation (59 ± 4% pre-trimming vs. 6 ± 1% post-trimming, $n = 156$, paired t-test, $\alpha < 0.05$, **Fig. 3D**), demonstrating the necessity of touch for localization.

To understand response diversity in the framework of whisker space, we quantified each neuron's response to GoW and LoW separately (10 mice, 529 neurons, **Fig. 3E**). Almost half of all neurons increased their firing rate during both GoW and LoW (251/529 neurons), while the remaining neurons increased their firing rate for one stimulus type yet decreased it for the other. To illustrate these effects, we plotted the population averaged firing rates of each response type relative to the onset of surface translation (**Fig. 3F**). Overall, these data demonstrate that SC neurons were highly sensitive to changes in whisker contacts, while showing relatively weak changes in firing rate during translations that sustained contact with the same whiskers (**Fig. 3G**).

The transient response emerges from externally generated changes in whisker contact

We hypothesized that the transient response selectively emerged from external, rather than self-generated changes in whisker contact. To test this hypothesis, we modified our experiment so that the surface periodically moved between rostral space and a location entirely outside the whisking field (**Fig 4A**). With the surface in rostral space, mice voluntarily lost and gained touch (Self LoW/GoW) with the surface as they periodically (7.2 ± 5.6 second interval) transitioned between resting (no running or touch) and locomotive whisking and touch (**Fig. 4B**). Importantly, this self-imposed interval between a loss and gain in whisker contact was similar in duration to

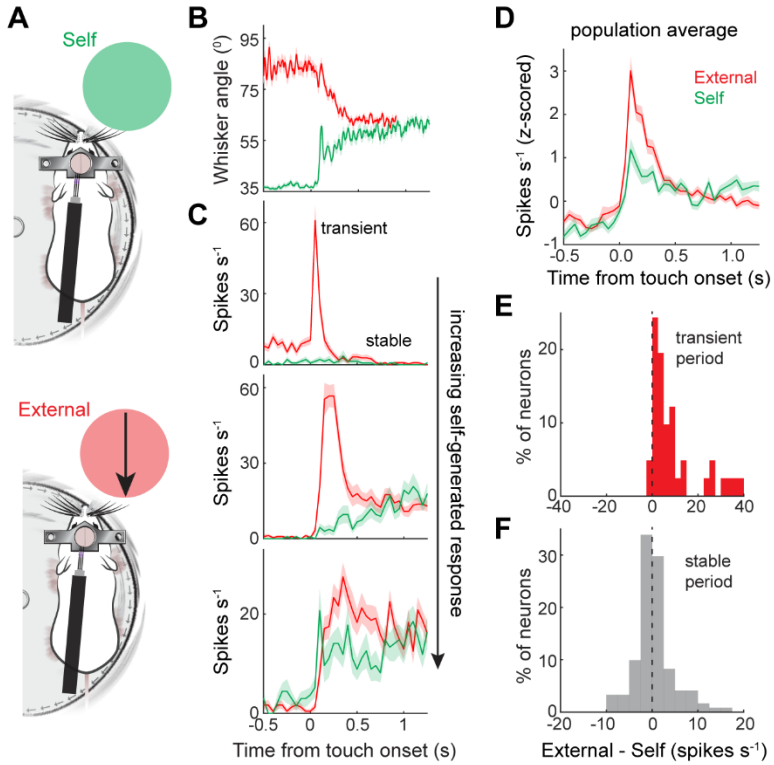

Figure 4. The transient response encodes externally generated changes in whisker contact
A) Experimental design comparing GoW from self-motion to GoW from external motion. **B**) Whisker angle during GoW induced by self- (green) and external motion (red). **C**) Firing rates of three example neurons aligned to the onset of self- and external GoW. Bottom, a neuron lacking a transient response with an equivalent response to external and self-GoW. **D**) Population averaged, z-scored firing rates aligned to the onset of external and self-GoW. **E**) Firing rates during the initial transient period were significantly greater from external GoW than from self-GoW ($p = 8e^{-5}$, 2 mice, 41 neurons). **F**) Firing rates during the later stable period were similar between trials with external and self-GoW ($p = 0.26$, 2 mice, 121 neurons). All values are mean ± s.e.m.

the interval between external surface translations (as discussed above). During self-generated gains in whisker contact, no transient response occurred, and neural activity was stable for as long as the mouse whisked against the surface. However, only when the surface translated into the whisking field did many neurons display a large and rapidly adapting transient response (**Fig. 4C, D**). Therefore, firing rates from external GoW were greater than self-GoW around the onset of touch (**Fig. 4E**, $p=8e^{-05}$, 41 neurons with transient, 2 mice), but rapidly equalized with adaptation of the externally generated transient response (**Fig. 4F**, $p = 0.26$, 121 neurons, 2 mice).

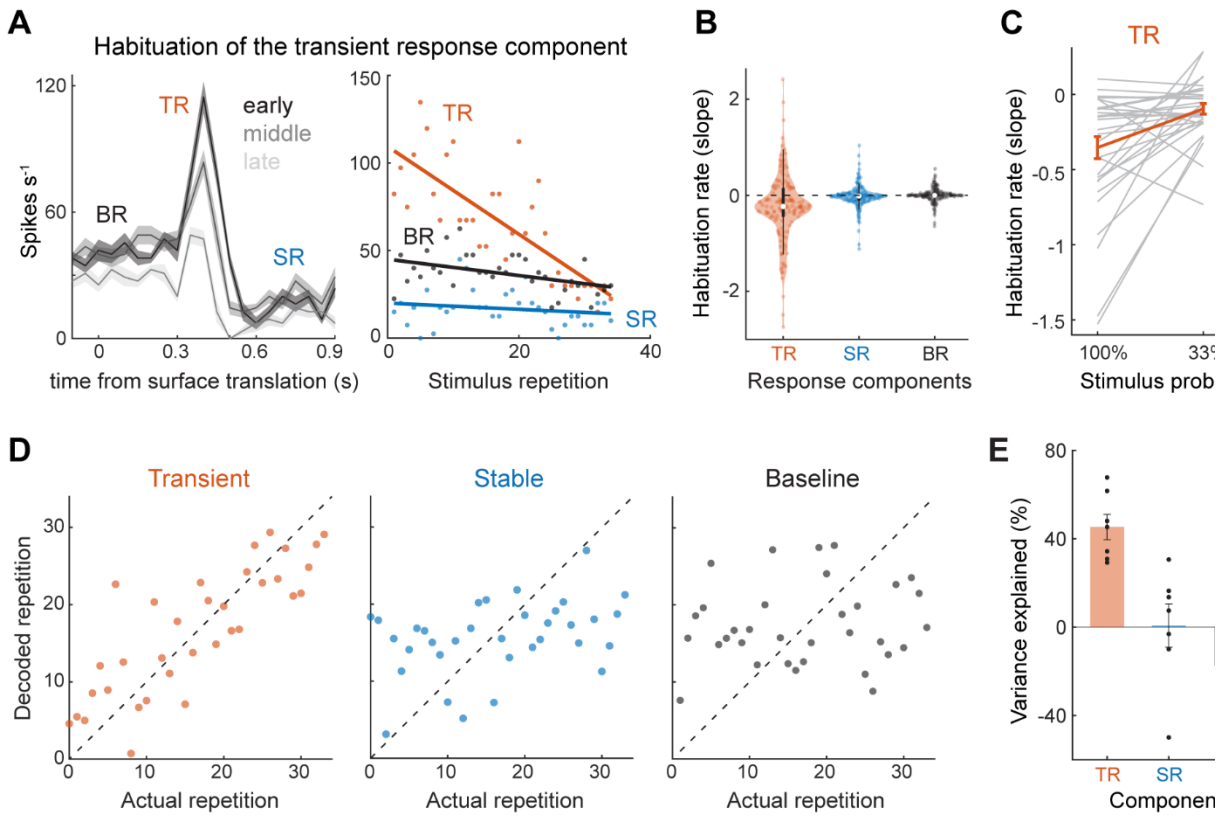

Figure 5. Sensory expectation controls the transient response
A) An example neuron displaying baseline (BR), transient (TR), and stable (SR) activity from GoW contact. The magnitude of each response component as a function of stimulus repetition (early: first third of trials, middle: second third; late: last third). **B**) Stimulus repetition slopes for neurons with a TR component that were significantly fit by a linear model ($p < 0.05$, t-test). Repetition slopes were calculated separately for the TR, SR, and BR periods (10 mice, 148 neurons). **C**) The rate of habituation based on stimulus probability (2 mice, 32 neurons with TR during both translations, sign rank $p = .0026$). **D**) Neural decoding of stimulus repetition using each of the response components. Scatter plots comparing the actual stimulus repetition to the neural decoded repetition from a single experiment. **E**) Decoder performance (variance explained) for the seven mice that accurately predicted stimulus repetition.

149 *Sensory expectation controls the transient response*

150 Next, we sought to determine if responses to externally generated whisker change were static
151 or modulated by higher-level stimulus features. To do so, we analyzed the effect of stimulus
152 repetition on the magnitude of SC responses. For each experiment, we selected trials with a
153 GoW translation and calculated the baseline (BR), transient (TR), and stable (SR) responses as
154 a function of stimulus repetition, as shown in one example neuron (**Fig. 5A**). Importantly, these
155 GoW stimuli were interleaved with other stimulus translations due to the random trial structure.
156 We discovered that TR magnitude decayed with increasing GoW repetitions while the SR and
157 BR components remained stable. This TR-specific habituation was consistent across the

population (**Fig. 5B**, 148 neurons, 10 mice, $p = 5.5e^{-5}$ for TR; p = 0.24 for SR; p = 0.74 for BR, t-test), and was unlikely caused by receptor-level adaptation, since the average interval between each GoW event was around one minute (67 ± 5 sec, 10 mice). Interestingly, habituation of the TR appeared to be controlled by expectation, as its rate was significantly higher for stimuli with 100% probability (return from rostral), in comparison to stimuli with only 33% probability (excursion from center, **Fig. 5C**, 32 TR neurons in 2 mice, p = 0.0026, signed rank).

Given the linear nature of habituation in SC neurons, we sought to determine if TR magnitude could encode the precise number of stimulus repetitions. Using an ANOVA with multiple comparisons, we identified the neurons in every mouse that contained a TR component (28 ± 8 neurons per mouse). Using a linear regression model with 5-fold cross-validation, we found that the TR component accurately predicted repetition number in seven of ten mice, while the BR and SR components of these same neural populations predicted repetition in only one mouse each (**Fig. 5D, E**, variance explained is 45 ± 6% for TR, 0.73 ± 10% for SR, -17 ± 9% for BR, 7 mice. See **suppl. Fig. 2**). Therefore, the TR incrementally decreased as a function of stimulus repetition, arguing that sensory expectations accumulate in SC neurons over many minutes.

Spike timing correlates with self-generated spatial features

Since surface translations engaging the same whiskers caused only modest changes in overall firing rate, we speculated that changes in spike timing may support spatial localization in the absence of somatotopic cues. To test this hypothesis, we first assessed the presence of a temporal code, by aligning SC spiking to the start of whisker protraction (**Fig. 6A, C**). Neurons displayed non-uniform patterns of activity, revealing the presence of a precise temporal structure embedded within their firing rate. To better understand the temporal structure of spiking in the context of whisking, we created spike-triggered averages of whisker phase (or phase tuning, **Fig. 6B, D,** see methods). A large fraction of neurons displayed phase distributions significantly different from chance, during both free whisking in air and against the surface (31 ± 4% free whisking, 6 mice, 154 neurons; 45 ± 4% surface whisking, 12 mice, 378 neurons).

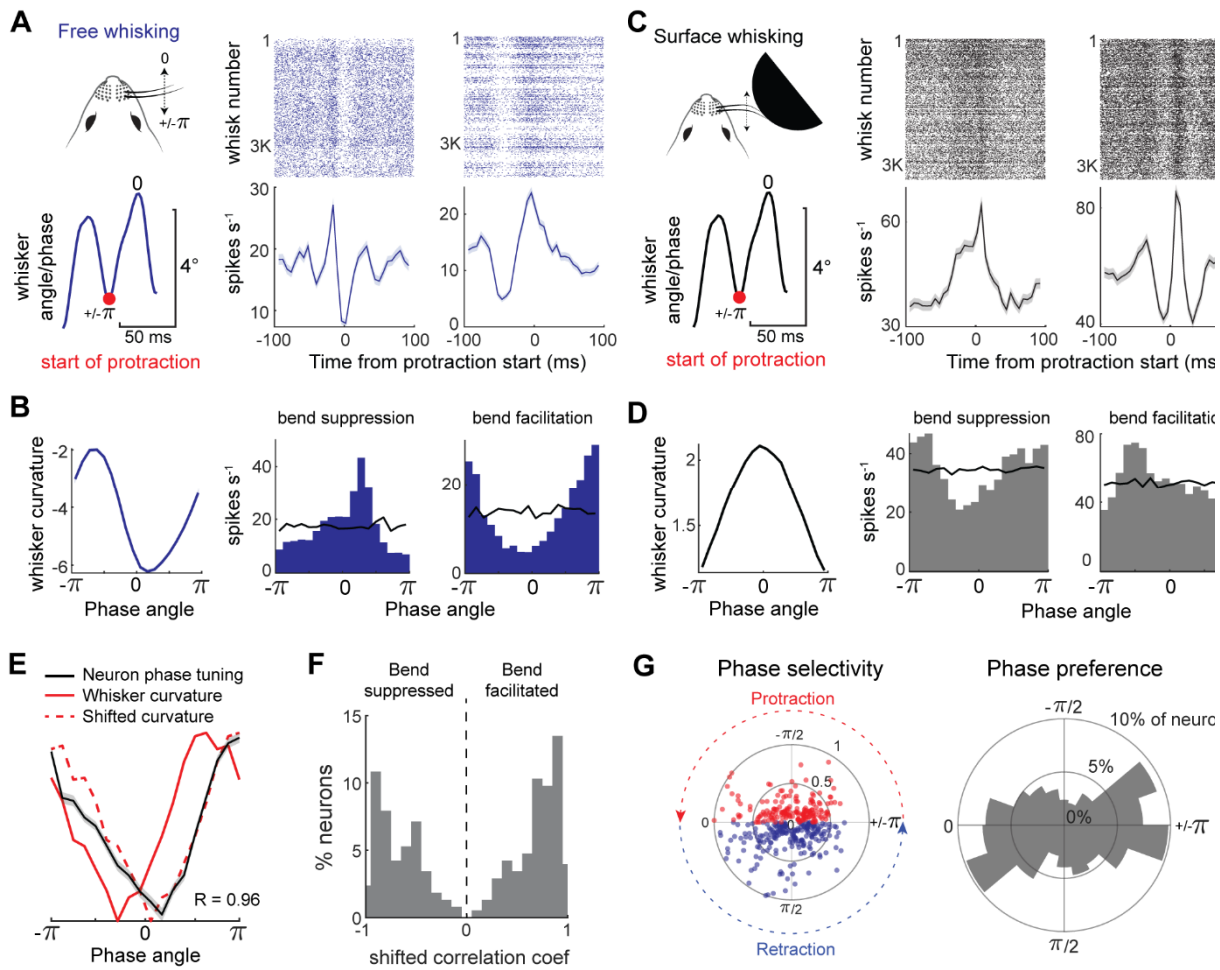

Figure 6. Spike timing correlates with self-generated spatial features
A) Left, schematic of the relationship between whisker angle and phase. The start of protraction is indicated by the red dot (± π). Right, spike rasters and mean firing rates aligned to the onset of whisker protraction during free whisking in air (two neurons). **B**) Left, whisker curvature as a function of phase (Curvature profile, mean ± s.e.m). Right, phase tuning (STAs) for the two neurons shown in panel A during free whisking in air. The black line illustrates each neuron's chance phase distribution (actual vs. chance: $p = 1e^{-218}$, $p = 3e^{-200}$, chi-squared goodness of fit). **C**, **D**) Same as A and B, except during surface whisking ($p = 5e^{-96}$, $p = 8e^{-82}$, chi-squared goodness of fit). **E**) Phase tuning of an example neuron, its temporally corresponding whisker curvature, and the phase-shifted curvature with the highest correlation coefficient. **F**) Histogram of the correlation between the phase-shifted curvature profile and the neuronal phase tuning (12 mice, 378 neurons). **G**) Phase selectivity of neuronal population and a histogram of their phase preferences (12 mice, 378 neurons, 45 ± 3% prefer protraction, 55 ± 3% prefer retraction).

Next, we observed that the increases in whisker curvature that occurred during protraction and the decreases that occurred during retraction were correlated with the shape of phase tuning (**Fig. 6 B, D**). In some neurons, we observed a striking resemblance between their phase tuning curve and the temporal profile of whisker curvature (**Fig. 6E**). To examine this relationship, we calculated the maximum correlation coefficient between each neuron's phase

tuning and the phase-shifted whisker curvature profile, to adjust for arbitrary differences in spike latency. The majority (213/378, 56%) of phase tuning curves were strongly (R > 0.7) correlated (bend facilitated) or strongly anti-correlated (bend suppressed) with increases in whisker curvature (**Fig. 6F**). Across the population, neurons primarily preferred phase angles shortly after the start of protraction or retraction **(Fig. 6G**), demonstrating a preference for either an increase or a decrease in curvature at the rapid timescale of a single whisk cycle.

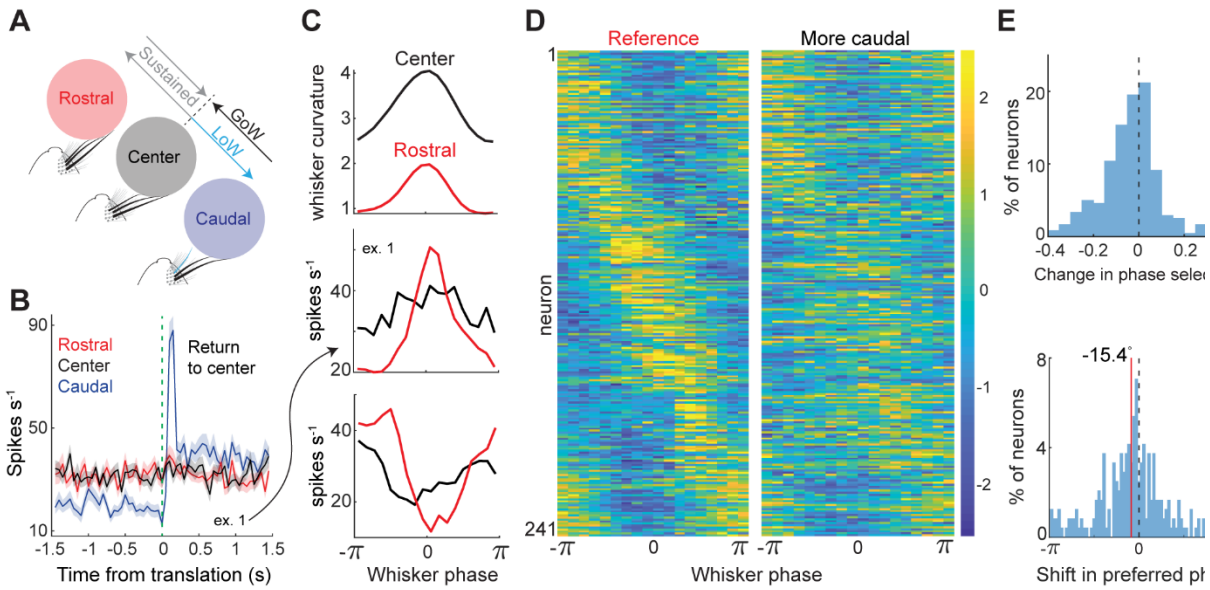

Figure 7. Shifts in spike timing encode changes in self-generated spatial features
A) Diagram illustrating sustained whisker contact for the rostral and center surface locations, and a loss of whisker contact for the caudal location. **B**) Example neuron demonstrating nearly identical firing rates for positions (rostral and center) with identical whiskers actively touching the surface. In the stable caudal location, the firing rate decreased, due to a loss of whisker contact. **C**) Curvature profiles (mean ± s.e.m) and their corresponding neuronal phase tuning for the same experiment in **B** at the center (black) and rostral (red) surface locations. **D**) Heatmap of z-scored phase tuning for neurons at two surface locations (8 mice, 241 neurons). **E**) Population histograms showing the change in phase selectivity ($p = 5e^{-7}$, paired t-test, 241 neurons) and the change in phase preference ($p = 0.006$, paired t-test) from translation into the more caudal location that contacted the same whisker(s).

Shifts in spike timing encode object locations that engage the same whiskers

Surface location had a profound effect on whisker curvature. We reasoned that if whisker curvature controls spike timing, then the phase tuning of neurons should shift in accordance with changes in the curvature profile. In an example neuron, we demonstrate how surface translation between the center and rostral locations elicited nearly identical firing rates, due to a lack of whisker change (**Fig. 7A**). When the surface translated from the rostral to the center

location, the profile of whisker curvature broadened, effectively shifting the curvature increase towards the start of protraction (**Fig. 7B**). This broadening of self-generated spatial features correlated with a decrease (broadening) in phase selectivity and a forward shift in phase preference, as shown in two example units. To illustrate this effect across the population, we compared phase tuning between two surface locations. In the more caudal location, phase selectivity significantly decreased ($p = 1e^{-7}$, paired-sample t test) while phase preference shifted towards the start of protraction ($p = 5.6e^{-3}$, paired-sample t test, **Fig. 7C, D**). Locomotion speed between surface locations was nearly identical, indicating that changes in running behavior were not the primary cause of this effect (**Suppl. Fig. 3**). Therefore, spike timing may help form a stable representation of object location using self-generated spatial cues.

Discussion

Navigation is a natural behavior that contextualizes incoming sensory stimuli with outgoing motor commands. To perform this feat, an internal model of self-motion is essential to recognize if changes in egocentric space originate from externally or internally generated movements (Ayaz et al., 2019; Jordan and Keller, 2020). By simulating whisker-guided navigation, we discovered that the mouse SC is specialized for locating unexpected, externally generated tactile motion. We identified a transient response (TR), found in many SC neurons, which selectively emerged during externally initiated touch and habituated in a context-specific manner. Habituation of the TR occurred independently of stable tactile responses in the same neurons, providing evidence for multiple distinct circuits controlling SC activity. Similar transient responses have been observed in intermediate-layer SC neurons responding to visual stimulation (Wang et al., 2022). However, in these cases, SC activity rapidly adapted to baseline, despite the persistence of visual stimulation. Therefore, stable sensory responses in the deep SC that persist for the entire duration of the stimulus may be a unique feature of active touch. Although, auditory SC responses to longer lasting (>150 ms) sounds have not yet been investigated, to our knowledge (Ito et al., 2020; Maldarelli et al., 2022).

Both the barrel cortex and brainstem provide monosynaptic sensory drive to SC neurons[16–18,25,]. How SC neurons balance these inputs with higher-order motor and associative signals to contextualize stimulus information remains an important topic. We hypothesize that an efference copy of whisker motion, possibly involving the cerebellum, motor cortex and brainstem, is critical for SC neurons to distinguish external from self-generated changes in tactile space (Alloway et al., 2010; Anderson et al., 2012; Kilteni and Henrik Ehrsson, 2020; Kojima and Soetedjo, 2018; Shadmehr et al., 2010; Singla et al., 2017). Value-coded output

from the basal ganglia could further shape the transient response in SC neurons to generate a neural mechanism for orienting towards novel or rewarding environmental cues (Jiang et al., 2003; Kaneda et al., 2008; J. Lee et al., 2020; Lee and Sabatini, 2021; Liu and Basso, 2008; Mcelvain et al., 2021; Villalobos et al., 2022). Importantly, mice in our study behaved voluntarily, and were not seeking reward. In this free-form context, habituation of the TR may reflect a central mechanism for ignoring stimuli of diminishing value (K. H. Lee et al., 2020; Tafreshiha et al., 2021). Whether this mechanism relies on changes in inhibitory signaling from the SNr or to the activity of local SC interneurons remains an important consideration (Essig et al., 2021; Kaneda et al., 2008; Sooksawate et al., 2011). In different behavioral contexts, goal-directed processing may flexibly control the TR to match the expected value of the target stimulus (Basso and Wurtz, 1998, 1997; Griggs et al., 2018; Zhang et al., 2021). While visual response habituation has been observed previously in primates and rodents (Boehnke et al., 2011; Cynader and Berman, 1972; Drager and Hubel, 1975; K. H. Lee et al., 2020), our study is the first to demonstrate habituation in the SC supporting somatosensory expectations.

Neuronal selectivity for externally generated stimulation has been observed in other sensory modalities and brain areas. Neurons in the monkey cerebellum selectively respond to external but not self-generated vestibular accelerations (Brooks and Cullen, 2013). Neurons in the monkey visual cortex display a unique window of suppression when voluntary eye-movements pass neuronal receptive fields through a visual object (Troncoso et al., 2015). Neurons in the superficial cortical layers selectively respond to mismatches between visual flow and locomotion speed (Jordan and Keller, 2020; Zmarz and Keller, 2016). In the auditory brainstem, neurons cancel self-generated sounds associated with licking (Singla et al., 2017), and neurons in the hindbrain of weakly electric fish cancel self-generated electric signals(Bell, 2001). We are the first to demonstrate a class of neurons in the superior colliculus that selectively respond to externally generated changes in space. Since changes in whisker contact were necessary for this response to emerge, the cancellation of self-generated touch is specific to each whisker.

SC population decoding of surface location was accurate only when its movement engaged different whiskers. This argues that a somatotopic map of whisker space is central to object localization in the SC. Given this result, one might assume that SC neurons can only encode coarse, whisker-level changes in space. However, we found that shifts in spike timing relative to self-generated tactile cues encode object locations that engage the same whiskers. The foundation for this claim is the strong correlation between neuronal phase tuning and the

temporal profile of whisker curvature. As the surface moved caudal, the profile of curvature broadened, leading to equivalent changes in spike timing. The circuit mechanisms underlying SC phase tuning are unknown, but inputs from both the brainstem and barrel cortex are candidates (Ebert et al., 2021; Isett and Feldman, 2020; Severson et al., 2017; Wallach et al., 2016). These somatosensory inputs to the SC spike primarily during periods of protraction, yet we discovered that half of SC neurons prefer the opposite phase (retraction). Under anesthesia, touch responses in the SC also spike exclusively during the protraction period (Bezdudnaya and Castro-Alamancos, 2014). Therefore, during awake, active touch, the SC may perform a novel computation (bend suppression) that enhances spike probability for periods opposite its cortical and brainstem inputs. Target-specific perturbations are needed to dissect the circuit mechanisms supporting this potentially unique form of phase tuning. While the observed shifts in spike timing may encode *changes* in surface location, an internal model of whisker position is ultimately necessary for decoding absolute distance in egocentric space (Cheung et al., 2019; Szwed et al., 2003). Nonetheless, our results establish spike timing in the SC as a potential mechanism for obtaining hyperacuity using an active sensor array (Knutsen et al., 2006).

Knowing the location of our body relative to surrounding objects is critical to daily life. We constantly adjust our hands, eyes, and posture to optimize the flow of sensory information while performing tasks. While doing so, the brain must differentiate these active sensing strategies from movements generated by external objects. Such computations are pervasive across sensory modalities and brain areas involved in sensorimotor processing. Neurons in the SC perform a unique computation for localizing unexpected, externally generated changes in space, while remaining sensitive to on-going, self-generated spatial features. It is perhaps surprising that single neurons in an ancient midbrain structure can multiplex this level of information. Given the diversity and complexity of signals that impinge upon the mammalian SC, this is perhaps expected, just as well. How the SC interprets this rich diversity of information to guide behavior remains an exciting and important topic.

Methods

Experimental Model and Subject Details

Mice of a CD-1 background of both sexes, between the ages of 9-15 weeks were used for all experiments. The Purdue Institutional Animal Care and Use Committee (IACUC) and the Laboratory Animal Program (LAP) approved all procedures. Mice were socially house with five

306 or less per cage and maintained in reverse light-dark cycle (12:12 hr.). All experiments were
307 conducted during the animal's subjective night.
308
309 *In-vivo Electrophysiology*
310 Prior to behavioral conditioning, a custom aluminum headplate was attached to each mouse to
311 enable head fixation. Briefly, animals were anesthetized under 5% isoflurane and maintained at
312 ~3% while monitoring body temperature and respiratory rate throughout the procedure. Artificial
313 tears ointment was applied to keep the eyes hydrated. The skin and fur over the skull were
314 disinfected with 70% ethanol followed by betadine and incised using sterilized surgical
315 instruments. A tissue adhesive (Liquivet) and dental cement (Metabond) was applied over the
316 skull and wound margins. The headplate was attached to the skull with dental cement. Lastly
317 buprenorphine (mg/kg) was administered as a postoperative analgesic. Two days after
318 headplate implantation, mice were placed on a circular treadmill for 1 hour per day for up to 10
319 days, or until they learned to run freely at a steady pace.
320 On the day of the electrophysiology recording, mice were briefly anesthetized to perform
321 a craniotomy over the SC. A 1mm diameter craniotomy was made using a biopsy punch
322 (Robbins Instruments) and then covered with a silicone gel (Dowsil). After 2-3 hours of recovery,
323 mice were placed in the experimental rig and a three-shank custom probe (Neuronexus) of 128-
324 channels was lowered into the brain using a micromanipulator (NewScale). After exiting the
325 ventral surface of the cortex, as evident by a loss of spiking, the electrode was lowered at a rate
326 of 75μm/min while constantly searching for activity driven by flashes of light. The onset of visual
327 activity was used to mark the depth of the SC surface (~1000μm below cortical surface). The
328 electrode was further lowered into the intermediate and deep layers, where manual whisker
329 deflections caused strong neuronal responses. The receptive field of neurons were mapped by
330 manually deflecting individual whiskers and locating the primary drivers of neuronal activity.
331 Whiskers that did not elicit detectable activity were trimmed. Recordings were targeted towards
332 the C-row and macrovibrissae. If the electrode penetration missed the target, it was removed
333 and re-inserted based on the coordinates of somatotopic space. In most experiments, mice had
334 3 – 5 intact whiskers contacting the surface, which spanned one or two rows. In other cases,
335 mice had two whiskers intact.
336
337 *Whisker guided virtual navigation*
338 The circular treadmill was attached to a digital encoder that drove the rotation of a tactile
339 surface in a closed-loop. A trial began after 200cm of locomotion on the treadmill to ensure the

mouse was actively sensing the surface. Shortly (1.4 sec.) after the trial began, the surface either translated 1 cm linear distance into rostral or caudal space or remained at the center/home location. Each outcome was randomly chosen with equal (33.33%) probability. In six mice, an additional location was added that was entirely outside the whisker field, giving each excursion a random 25% probability. While at the rostral/caudal position, mice had to run an additional 200cm before the surface would return to the center. An opaque flag over the eye and white background noise obscured visual and auditory cues, respectively.

We modified the translations for two mice to record responses during self- and external-GoW. The surface translated between two locations: rostral or entirely outside the whisking field. The average interval between translations was 20.3 ± 3 seconds, while the average interval between two successive translations resulting in external-GoW was 74.6 ± 0.6 seconds. The standard deviation of the interval between translations was 12.8 seconds, due to variation in mouse locomotion speed. External-GoW occurred when the surface translated into the whisking field while the mouse was locomoting. Self-motion alone occurred when the surface was outside the whisking field, and mice transitioned from resting to locomotive whisking in air periodically. Self-GoW occurred when the surface was stationary in the whisking field, allowing periodic bouts of self-motion to induce surface whisking.

Whisker Tracking & kinematics

Whiskers were tracked at 500fps during the trial. A high-speed infrared camera (Photonfocus DR1) and a mirror angled at 45 degrees captured whisker motion under IR illumination. Videos were synchronized with neural data via external triggers generated by a National Instruments card and recorded on an Intan 512 controller. DeepLabCut was used to label the whisker(s) and track their movement(Mathis et al., 2018). Four evenly spaced points on each whisker were labeled. Approximately 150 frames were manually labeled from each experiment spanning all surface positions. The DLC neural network was trained for at least 200k iterations and the final labels were manually checked for accuracy. Whisker position/angle was calculated for each label on each whisker with reference to a user defined point on the face relative to the frame's vertical axis. Whisker bend/curvature was calculated from the three distal labels on each whisker using Menger curvature. The whisker bend derivative was calculated as the local slope with cubic approximation in a moving window of 100ms. Whisker angle was bandpass filtered (1-30Hz, fdesign.bandpass order 4, MATLAB), Hilbert transformed (hilbert, MATLAB), and the phase angle was obtained from the complex value (angle, MATLAB). A phase angle of zero depicts the most protracted angle, while +/- π was the most retracted angle.

Spike Sorting

Spikes sorting was performed using the Kilosort2(Pachitariu et al., 2016) and manually curated using Phy2 gui (https://github.com/cortex-lab/phy). Spike clusters were considered single units based on their spike waveform, location on the electrode, and cross-correlogram of spike times. Single units were used for all analyses in the paper.

Statistical Analysis

Location classifier

To classify the location of the tactile surface from population-level SC activity, we applied the Neural Decoding Toolbox(Meyers, 2013) using a support vector machine (SVM). The classifier predicted surface location (rostral, caudal, center) throughout the duration of the trial. Only responsive neurons for surface translation were used. Spike data was first Z-scored to prevent high firing rate neurons from having a disproportionate influence on classification. The spike rate of every neuron was calculated using 150ms bins and surface location was predicted every 20ms to plot classification accuracies over time. A 10-fold cross validation was performed along with 50 resample runs to calculate a robust estimate of classification accuracies. The classification accuracy was measured based on the zero-one loss function.

Modulation Indices

All modulation indices (RMI, CMI, GoW, LoW) were calculated as the difference divided by the sum of spike rate averages in a 500 ms bin during the translation and the baseline period. To measure the discriminability between rostral and caudal translations, we measured the distance value (d-value) which is the distance of a point from the line of unity on the RMI CMI plot.

Transient (TR), Stable (SR), and Baseline (BR) response components:

A translation was defined as a GoW/LoW when at least one whisker gained or lost contact with the surface. Trials with sustained touch maintained contact with the same whiskers during surface translation. Since changes in whisker space (GoW/LoW) happened at slight time differences relative to the onset of translation across mice, we selected a custom window for the TR for each mouse based on the population average firing rate for every whisker change translation. We verified this window onset with kinematic analysis of high-speed videos. The SR was calculated 1.0 – 1.4 seconds after the start of translation, while BR was calculated in the 400ms window before the start of translation for all analysis. When aligning spikes to whisker

protraction in the SR period (Fig 2F), the SR window was chosen as .4 seconds before the start of the next translation, that is the most adapted stable period. We performed a one-way ANOVA (MATLAB function anova1) on the BR, TR, and the SR windows for every neuron. A Tukey post hoc test (multcompare, MATLAB) was used to test for significant ($\alpha < 0.05$) differences between the BR, TR, and SR. Neurons with significantly different TR and/or SR from BR were called tactile responsive neurons and used for all analyses. TR neurons had a mean firing rate during the initial response window that was significantly greater than the BR and SR.

Stimulus repetition

To obtain repetition slopes, we fit firing rates of TR neurons in the TR, SR and BR window with a linear regression model using the MATLAB fitlm function. Only neurons with a significant linear fit were included in the population analysis.

To decode repetition number, we used all TR neurons that did not drift. Neuronal drift was determined by testing if the baseline firing rate during the first 10 trials was different from the last 10 trials using a Wilcoxon signed rank test. The firing rate of the selected neurons within the TR, SR, and BR windows was then used to predict the repetition number using the SVM regression (fitrsvm, MATLAB) with 5-fold cross validation where the model is trained and tested on different data sets. Prediction accuracy was reported as percent variance explained. In the below equation, R^2 is the fraction of variance explained, $\hat{y}_i$ are the predicted values, y_i are the true values, and $\bar{y}$ is the mean value of true values.

$$R^2 = 1 - \frac{\sum_i (\hat{y}_i - y_i)^2}{\sum_i (y_i - \bar{y})^2}$$

Self-GoW and external-GoW

Self-GoW and external-GoW was calculated in the transient and the stable window. Self-GoW was calculated as a difference between mean firing rates during self-GoW and self-motion. External-GoW was calculated during surface translation as the difference between the mean firing rates during the TR/SR and baseline window.

Phase tuning

To obtain each neuronal phase tuning curves, we generated spike triggered averages of whisker phase (STA). Spike counts for each neuron were binned into 20^0 non-overlapping phase bins spanning from – π to +π, determined by the phase angle at the time of each spike. To calculate firing rate, spike counts in each phase bin was divided by time the whiskers spent

at each angle. Neurons were considered phase tuned if their firing rate distribution of phase (STA) was significantly different from a chance distribution (χ^2 goodness of fit, $\alpha < .05$). The phase preference of each neuron was the circular mean of its phase tuning curve(Berens, 2009), while the phase selectivity was the modulation depth, which was the difference divided by the sum of maximum and minimum STA firing rates.

Acknowledgements

Authors would like to acknowledge the members of the Pluta lab, Kate Hong, Ed Bartlett and Daniel Butts for providing valuable feedback on the manuscript.

Competing Interest

The authors declare no competing interest

References

Allen KM, Lawlor J, Salles A, Moss CF. 2021. Orienting our view of the superior colliculus: specializations and general functions. *Curr Opin Neurobiol*. doi:10.1016/j.conb.2021.10.005

Alloway KD, Smith JB, Beauchemin KJ. 2010. Quantitative analysis of the bilateral brainstem projections from the whisker and forepaw regions in rat primary motor cortex. *J Comp Neurol* **518**:4546–4566. doi:10.1002/cne.22477

Anderson SR, Porrill J, Pearson MJ, Pipe AG, Prescott TJ, Dean P. 2012. An Internal Model Architecture for Novelty Detection: Implications for Cerebellar and Collicular Roles in Sensory Processing. *PLoS One* **7**:e44560. doi:10.1371/journal.pone.0044560

Aronoff R, Matyas F, Mateo C, Ciron C, Schneider B, Petersen CCHH. 2010. Long-range connectivity of mouse primary somatosensory barrel cortex. *Eur J Neurosci* **31**:2221–2233. doi:10.1111/j.1460-9568.2010.07264.x

Ayaz A, Stäuble A, Hamada M, Wulf MA, Saleem AB, Helmchen F. 2019. Layer-specific integration of locomotion and sensory information in mouse barrel cortex. *Nat Commun* **10**. doi:10.1038/s41467-019-10564-8

Basso MA, May PJ. 2017. Circuits for Action and Cognition: A View from the Superior Colliculus. *Annu Rev Vis Sci* **3**:197–226. doi:10.1146/annurev-vision-102016-061234

Basso MA, Wurtz RH. 1998. Modulation of neuronal activity in superior colliculus by changes in target probability. *J Neurosci* **18**:7519–7534. doi:10.1523/jneurosci.18-18-07519.1998

Basso MA, Wurtz RH. 1997. Modulation of neuronal activity by target uncertainty. *Nature* **389**:66–69. doi:10.1038/37975

Bell CC. 2001. Memory-based expectations in electrosensory systems. *Curr Opin Neurobiol*. doi:10.1016/S0959-4388(00)00238-5

Berens P. 2009. CircStat : A MATLAB Toolbox for Circular Statistics. *J Stat Softw* **31**:1–21. doi:10.18637/jss.v031.i10

Bezdudnaya T, Castro-Alamancos MA. 2014. Neuromodulation of whisking related neural activity in superior colliculus. *J Neurosci* **34**:7683–7695. doi:10.1523/JNEUROSCI.0444-14.2014

Bezdudnaya T, Castro-Alamancos MA. 2011. Superior colliculus cells sensitive to active touch and texture during whisking. *J Neurophysiol* **106**:332–346. doi:10.1152/jn.00072.2011

Boehnke SE, Berg DJ, Marino RA, Baldi PF, Itti L, Munoz DP. 2011. Visual adaptation and novelty responses in the superior colliculus. *Eur J Neurosci* **34**:766–779. doi:10.1111/j.1460-9568.2011.07805.x

Brooks JX, Cullen KE. 2013. The primate cerebellum selectively encodes unexpected self-motion. *Curr Biol* **23**:947–955. doi:10.1016/j.cub.2013.04.029

Cang J, Savier E, Barchini J, Liu X. 2018. Visual Function, Organization, and Development of the Mouse Superior Colliculus 1–24. doi:10.1146/annurev-vision-091517

Castro-Alamancos MA, Favero M. 2016. Whisker-related afferents in superior colliculus. *J Neurophysiol* **115**:2265–2279. doi:10.1152/jn.00028.2016

Cheung J, Maire P, Kim J, Sy J, Hires SA, Object A, Cheung J, Maire P, Kim J, Sy J, Cheung J, Maire P, Kim J, Sy J, Hires SA. 2019. The Sensorimotor Basis of Whisker-Guided Anteroposterior Object Localization in Head-Fixed Mice. *Curr Biol* 1–12. doi:10.1016/j.cub.2019.07.068

Cohen JD, Castro-Alamancos MA. 2010. Behavioral state dependency of neural activity and sensory (whisker) responses in superior colliculus. *J Neurophysiol* **104**:1661–1672. doi:10.1152/jn.00340.2010

Cohen JD, Hirata A, Castro-Alamancos MA. 2008. Vibrissa sensation in superior colliculus: Wide-field sensitivity and state-dependent cortical feedback. *J Neurosci* **28**:11205–11220. doi:10.1523/JNEUROSCI.2999-08.2008

Cynader M, Berman N. 1972. Receptive-field organization of monkey superior colliculus. *J Neurophysiol* **35**:187–201. doi:10.1152/jn.1972.35.2.187

Drager UC, Hubel DH. 1976. Topography of visual and somatosensory projections to mouse superior colliculus. *J Neurophysiol* **39**:91–101. doi:10.1152/jn.1976.39.1.91

Drager UC, Hubel DH. 1975. Responses to visual stimulation and relationship between visual, auditory, and somatosensory inputs in mouse superior colliculus. *J Neurophysiol* **38**:690–713. doi:10.1152/jn.1975.38.3.690

Duan CA, Pagan M, Piet AT, Kopec CD, Akrami A, Riordan AJ, Erlich JC, Brody CD. 2021. Collicular circuits for flexible sensorimotor routing. *Nat Neurosci* **24**:1110–1120. doi:10.1038/s41593-021-00865-x

Ebert C, Bagdasarian K, Haidarliu S, Ahissar E, Wallach A. 2021. Interactions of whisking and touch signals in the rat brainstem. *J Neurosci* **41**:4826–4839. doi:10.1523/JNEUROSCI.1410-20.2021

Essig J, Hunt JB, Felsen G. 2021. Inhibitory neurons in the superior colliculus mediate selection of spatially-directed movements. *Commun Biol* **4**. doi:10.1038/s42003-021-02248-1

Evans DA, Stempel AV, Vale R, Ruehle S, Lefler Y, Branco T. 2018. A synaptic threshold mechanism for computing escape decisions. *Nature* **558**:590–594. doi:10.1038/s41586-018-0244-6

Griggs WS, Amita H, Gopal A, Hikosaka O. 2018. Visual neurons in the superior colliculus discriminate many objects by their historical values. *Front Neurosci* **12**:396. doi:10.3389/fnins.2018.00396

Hikosaka O, Wurtz RH. 1985. Modification of saccadic eye movements by GABA-related substances. I. Effect of muscimol and bicuculline in monkey superior colliculus. *J Neurophysiol* **53**:266–291. doi:10.1152/jn.1985.53.1.266

Hoy JL, Yavorska I, Wehr M, Niell CM. 2016. Vision Drives Accurate Approach Behavior during Prey Capture in Laboratory Mice. *Curr Biol* **26**:3046–3052. doi:10.1016/j.cub.2016.09.009

Huang M, Li D, Cheng X, Pei Q, Xie Z, Gu H, Zhang X, Chen Z, Liu A, Wang Y, Sun F, Li Y, Zhang J, He M, Xie Y, Zhang F, Qi X, Shang C, Cao P. 2021. The tectonigral pathway regulates appetitive locomotion in predatory hunting in mice. *Nat Commun* **12**:1–17. doi:10.1038/s41467-021-24696-3

Isett BR, Feldman DE. 2020. Cortical Coding of Whisking Phase during Surface Whisking. *Curr Biol* **30**:1–10. doi:10.1016/j.cub.2020.05.064

Ito S, Si Y, Feldheim DA, Litke AM. 2020. Spectral cues are necessary to encode azimuthal auditory space in the mouse superior colliculus. *Nat Commun* **11**. doi:10.1038/s41467-020-14897-7

Jiang H, Stein BE, McHaffie JG. 2003. Opposing basal ganglia processes shape midbrain visuomotor activity bilaterally. *Nature* **423**:982–986. doi:10.1038/nature01698

Jordan R, Keller GB. 2020. Opposing Influence of Top-down and Bottom-up Input on Excitatory Layer 2/3 Neurons in Mouse Primary Visual Cortex. *Neuron* **108**:1194-1206.e5. doi:10.1016/j.neuron.2020.09.024

Kaneda K, Isa K, Yanagawa Y, Isa T. 2008. Nigral inhibition of GABAergic neurons in mouse superior colliculus. *J Neurosci* **28**:11071–11078. doi:10.1523/JNEUROSCI.3263-08.2008

Kilteni K, Henrik Ehrsson H. 2020. Functional connectivity between the cerebellum and somatosensory areas implements the attenuation of self-generated touch. *J Neurosci* **40**:894–906. doi:10.1523/JNEUROSCI.1732-19.2019

Knutsen PM, Pietr M, Ahissar E. 2006. Haptic object localization in the vibrissal system: behavior and performance. *J Neurosci* **26**:8451–64. doi:10.1523/JNEUROSCI.1516-06.2006

Kojima Y, Soetedjo R. 2018. Elimination of the error signal in the superior colliculus impairs saccade motor learning. *Proc Natl Acad Sci U S A* **115**:E8987–E8995. doi:10.1073/pnas.1806215115

Lee J, Sabatini BL. 2021. Striatal indirect pathway mediates exploration via collicular competition. *Nature* **599**:645–649. doi:10.1038/s41586-021-04055-4

Lee J, Wang W, Sabatini BL. 2020. Anatomically segregated basal ganglia pathways allow parallel behavioral modulation. *Nat Neurosci* **23**:1388–1398. doi:10.1038/s41593-020-00712-5

Lee KH, Tran A, Turan Z, Meister M. 2020. The sifting of visual information in the superior colliculus. *Elife* **9**. doi:10.7554/eLife.50678

Liu P, Basso MA. 2008. Substantia nigra stimulation influences monkey superior colliculus neuronal activity bilaterally. *J Neurophysiol* **100**:1098–1112. doi:10.1152/JN.01043.2007/ASSET/IMAGES/LARGE/Z9K0080890180009.JPEG

Maldarelli G, Firzlaff U, Kettler L, Ondracek JM, Luksch H. 2022. Two Types of Auditory Spatial Receptive Fields in Different Parts of the Chicken's Midbrain. *J Neurosci* **42**:4669–4680. doi:10.1523/JNEUROSCI.2204-21.2022

Mathis A, Mamidanna P, Cury KM, Abe T, Murthy VN, Mathis MW, Bethge M. 2018. DeepLabCut: markerless pose estimation of user-defined body parts with deep learning. *Nat Neurosci* **21**:1281–1289. doi:10.1038/s41593-018-0209-y

Mcelvain LE, Chen Y, Moore JD, Lim BK, Costa RM, Kleinfeld D. 2021. Specific populations of basal ganglia output neurons target distinct brain stem areas while collateralizing throughout the diencephalon In brief. *Neuron* **109**:1–18. doi:10.1016/j.neuron.2021.03.017

Meyers EM. 2013. The neural decoding toolbox. *Front Neuroinform* **7**:8. doi:10.3389/fninf.2013.00008

Munoz DP, Wurtz RH. 1993. Fixation cells in monkey superior colliculus. II. Reversible activation and deactivation. *J Neurophysiol* **70**:576–589. doi:10.1152/jn.1993.70.2.576

Nagy A, Kruse W, Rottmann S, Dannenberg S, Hoffmann KP. 2006. Somatosensory-Motor Neuronal Activity in the Superior Colliculus of the Primate. *Neuron* **52**:525–534. doi:10.1016/j.neuron.2006.08.010

Pachitariu M, Steinmetz N, Kadir S, Carandini M, Harris KD. 2016. Kilosort: realtime spike-sorting for extracellular electrophysiology with hundreds of channels. *bioRxiv* 061481. doi:10.1101/061481

Severson KS, Xu D, Van de Loo M, Bai L, Ginty DD, O'Connor DH. 2017. Active Touch and Self-Motion Encoding by Merkel Cell-Associated Afferents. *Neuron* **94**:666-676.e9. doi:10.1016/j.neuron.2017.03.045

Shadmehr R, Smith MA, Krakauer JW. 2010. Error correction, sensory prediction, and adaptation in motor control. *Annu Rev Neurosci*. doi:10.1146/annurev-neuro-060909-153135

Shang C, Liu A, Li D, Xie Z, Chen Z, Huang M, Li Y, Wang Y, Shen WL, Cao P. 2019. A subcortical excitatory circuit for sensory-triggered predatory hunting in mice. *Nat Neurosci* **22**:909–920. doi:10.1038/s41593-019-0405-4

Singla S, Dempsey C, Warren R, Enikolopov AG, Sawtell NB. 2017. A cerebellum-like circuit in the auditory system cancels responses to self-generated sounds. *Nat Neurosci* **20**:943–950. doi:10.1038/nn.4567

Sommer MA, Wurtz RH. 2002. A pathway in primate brain for internal monitoring of movements. *Science (80-)* **296**:1480–1482. doi:10.1126/science.1069590

Sooksawate T, Isa K, Behan M, Yanagawa Y, Isa T. 2011. Organization of GABAergic inhibition in the motor output layer of the superior colliculus. *Eur J Neurosci* **33**:421–432. doi:10.1111/j.1460-9568.2010.07535.x

Szwed M, Bagdasarian K, Ahissar E. 2003. Encoding of vibrissal active touch. *Neuron* **40**:621–630. doi:10.1016/S0896-6273(03)00671-8

Tafreshiha A, Burg SAV, Smits K, Blomer LA, Heimel JA. 2021. Visual stimulus-specific habituation of innate defensive behaviour in mice. *J Exp Biol* **224**. doi:10.1242/JEB.230433/VIDEO-2

Troncoso XG, McCamy MB, Jazi AN, Cui J, Otero-Millan J, MacKnik SL, Costela FM, Martinez-Conde S. 2015. V1 neurons respond differently to object motion versus motion from eye movements. *Nat Commun* **6**:1–10. doi:10.1038/ncomms9114

Villalobos CA, Correspondence MAB, Basso MA. 2022. Optogenetic activation of the inhibitory nigro-collicular circuit evokes contralateral orienting movements in mice. *Cell Rep* **39**:110699. doi:10.1016/J.CELREP.2022.110699

Wallach A, Bagdasarian K, Ahissar E. 2016. On-going computation of whisking phase by mechanoreceptors. *Nat Neurosci* **19**:487–93. doi:10.1038/nn.4221

Wang L, Herman JP, Krauzlis RJ. 2022. Neuronal modulation in the mouse superior colliculus during covert visual selective attention. *Sci Rep* **12**. doi:10.1038/s41598-022-06410-5

Wise SP, Jones EG. 1977. Somatotopic and columnar organization in the corticotectal projection of the rat somatic sensory cortex. *Brain Res* **133**:223–235. doi:10.1016/0006-8993(77)90760-0

Zhang B, Kan JYY, Yang M, Wang X, Tu J, Dorris MC. 2021. Transforming absolute value to categorical choice in primate superior colliculus during value-based decision making. *Nat Commun* **12**:1–14. doi:10.1038/s41467-021-23747-z

Zmarz P, Keller GB. 2016. Mismatch Receptive Fields in Mouse Visual Cortex. *Neuron* **92**:766–772. doi:10.1016/j.neuron.2016.09.057